Applied Catalysis B: Environmental 244 (2019) 671–683

Contents lists available at ScienceDirect

Applied Catalysis B: Environmental

journal homepage: www.elsevier.com/locate/apcatb

Improved activity and significant SO_2 tolerance of samarium modified CeO_2-TiO_2 catalyst for NO selective catalytic reduction with NH_3

Hao Liu[a,b], Zhongxuan Fan[a], Chuanzhi Sun[a,b,*], Shuohan Yu[a], Shuai Feng[c], Wei Chen[b], Dezhan Chen[b], Changjin Tang[a], Fei Gao[a], Lin Dong[a,*]

[a] School of the Environment, Jiangsu Key Laboratory of Vehicle Emissions Control, Center of Modern Analysis, Nanjing University, Nanjing 210093, PR China
[b] College of Chemistry, Chemical Engineering and Materials Science, Shandong Provincial Key Laboratory of Clean Production of Fine Chemicals, Institute of Materials and Clean Energy, Shandong Normal University, Jinan 250014, PR China
[c] College of Chemistry and Chemical Engineering, Taishan University, Taian 271021, PR China

A R T I C L E I N F O

Keywords:
NH_3-SCR
CeO_2-TiO_2 mixed oxide
Sm-doped catalyst
SO_2 tolerance

A B S T R A C T

The Sm doped CeO_2-TiO_2 mixed oxide catalyst, which exhibited excellent activity and tolerance to H_2O and SO_2 in the NH_3-SCR reaction, was synthesized. The reasons for the high activity and SO_2 resistance of the catalyst were investigated by a series of characterization. The H_2-TPR and O_2-TPD results suggested that the reducibility and oxygen storage capacity (OSC) of CeTi catalyst were promoted by the addition of Sm species, which was beneficial for improving the activity of catalyst. The *in situ* DRIFTS results revealed that the adsorptive ability of NO_x species and activation ability of NH_3 were enhanced by Sm doping, which was also propitious to enhance the activity. XPS combined with DFT calculated results confirmed that the transfer of electron by $Sm^{2+} + Ce^{4+} \rightleftharpoons Sm^{3+} + Ce^{3+}$ circles occurred in the SmCeTi catalyst. The redox circles may be the reason of the good SO_2 tolerance of the SmCeTi catalyst, for which suppressed the electron transferring from adsorbed SO_2 to Ce^{4+}. Through *in situ* DRIFTS and TG-DSC results, it can be concluded that the sulphation of catalyst was lowered by samarium doping into CeTi catalyst. Consequently, the SmCeTi catalyst exhibited significant SO_2 tolerance ability.

1. Introduction

Selective catalytic reduction of NO with NH_3 (NH_3-SCR) is a well-established technology for reducing NO from stationary sources (such as coal-fired power plants) [1–4]. V_2O_5-WO_3/TiO_2 catalysts have long been commercially experienced because they exhibit high SCR activity, thermal stability, and resistance to SO_2 poisoning [5–7]. Simultaneously, the NH_3-SCR reaction mechanism of V_2O_5-WO_3/TiO_2 catalyst has been systematically proposed by researchers [8,9]. Nevertheless, some inevitable disadvantages still exist, such as the narrow operating temperature window (300–420 °C), the biological toxicity of the catalysts and large amounts of N_2O generated, etc [10,11]. Therefore, development of non-vanadium catalysts with high catalytic activity for the NH_3-SCR reaction in a broader temperature range is urgent. Some new environmentally benign transition metal oxide-based catalysts such as Mn-based [12–15], Ce-Sn [16], Ce-Zr [17–19] and Ce-Ti [2,20–22] catalysts with evaluated deNO_x activity have been widely studied to find potential alternatives.

The Ce-Ti-based catalysts have attracted extensive attention for their high deNO_x efficiency and N_2 selectivity in NH_3-SCR reaction in a broad temperature range [23]. Li et al. [24] reported that Ce-Ti amorphous oxides showed superior NO conversion efficiency and good N_2 selectivity, and suggested that the Ce-O-Ti species were the active sites in NH_3-SCR reaction. Although the Ce-Ti catalyst possess a certain ability of SO_2 and H_2O resistance, unfortunately, the catalyst still suffers from deactivation by SO_2 and H_2O when the run duration is long, which limited its practical application [25]. Addition of modification agent to Ce-Ti mixed oxide is an efficient way to improve the activity and SO_2 tolerance of the catalyst. Liu et al. [26] studied the cobalt-doped Ce-Ti mixed oxide, over which ~100% NO conversion was reached at 200 °C, and the SO_2 tolerance ability of CoCeTi catalyst was distinctly enhanced. Shu et al. [27] reported that nearly 100% NO conversion was maintained for 12 h in the presence of 500 ppm SO_2 at 250 °C for the Fe-modified Ce-Ti catalyst. Zhang et al. [20] researched that the SnCeTi catalyst prepared by solvothermal method showed high NO conversion from 180 °C to 460 °C and excellent SO_2 resistance at

* Corresponding authors at: School of the Environment, Jiangsu Key Laboratory of Vehicle Emissions Control, Center of Modern Analysis, Nanjing University, Nanjing 210093, PR China.
E-mail addresses: suncz@sdnu.edu.cn (C. Sun), donglin@nju.edu.cn (L. Dong).

https://doi.org/10.1016/j.apcatb.2018.12.001
Received 1 August 2018; Received in revised form 12 November 2018; Accepted 1 December 2018
Available online 01 December 2018
0926-3373/

300 °C.

Rare earth elements are often used as catalyst or promoter of the catalyst [28]. In recent years, it is found that Sm-doped Mn-based catalysts exhibited considerably enhanced catalytic activity and H_2O/SO_2 tolerance in NH_3-SCR reaction [5,29,30]. For example, Meng et al. prepared the Sm-modified MnO_x catalyst and proposed that doping of Sm to MnO_x induced the bulk-like sulfate forming on the Sm sites and the Mn sites were protected consequently [29]. Here, in our work, samarium is used to modify the Ce-Ti mixed oxide catalysts and their catalytic performances for NH_3-SCR reaction are investigated. The H_2O or/and SO_2 resistance abilities of the catalysts are also evaluated. The focus of this work is to study the influences of Sm doping on the redox properties and surface acidity of catalysts, and further reveal the relationships between the surface physicochemical properties and the activities. The interaction mechanisms of reactant gas (such as NH_3, NO + O_2, NO + O_2 + NH_3 and SO_2 + O_2) with the surfaces of catalyst are systematically studied. In addition, the reason for the excellent SO_2 durability property of catalysts has also been thoroughly investigated.

2. Experimental

2.1. Catalyst preparation

All the catalysts we studied were synthesized by inverse co-precipitation method using the corresponding salt solutions. In detail, a certain amount of $Ti(SO_4)_2$, $Ce(NO_3)_3{\cdot}6H_2O$, $Sm(NO_3)_3{\cdot}6H_2O$ were dissolved in distilled water and stirred for 1 h to mix them uniformly, and then the mixed solution was slowly dropped in the excess ammonia (25 wt.%) with vigorously stirring for 5 h. After aging 24 h, the resulting suspension was filtered and washed by distilled water for 5 times. Then the obtained samples were dried at 110 °C for 12 h and calcined at 500 °C in flowing air for 4 h. These synthesized samples are denoted as SmTi, CeTi, SmCeTi (Sm: Ce: Ti = 0.1:0.3:1 mol ratio). Besides, the catalysts after NH_3-SCR reaction with the 32 h SO_2 resistance test are labeled as X-U, for example, CeTi catalyst is denoted as CeTi-U.

In addition, NH_4HSO_4 (5 wt.%) was supported on CeTi and SmCeTi by impregnation method. The obtained samples are denoted as CeTi-N and SmCeTi-N.

2.2. Catalyst characterization and density functional theory (DFT) calculations

Inductively coupled plasma-optical emission spectrometry (ICP-OES) was performed on a Thermo Scientific iCAP 7000 apparatus to determine the chemical composition of the samples. The specific surface areas of the catalysts were measured on a Micrometrics ASAP-2020 analyzer using Brunauer − Emmett − Teller (BET) method by nitrogen adsorption at 77 K. Before the adsorption measurement, approximately 0.1 g of sample was firstly degassed in a N_2/He mixture at 300 °C for 4 h. The Barrett − Joyner − Halenda (BJH) algorithm was employed to calculate the pore size distributions from the desorption branch of N_2 adsorption isotherm. Raman spectra were collected on a Spex 1877 D triplemate spectrograph with 2 cm^{-1} resolution at room temperature. The excitation source was a 532 nm DPSS diode-pump solid semiconductor laser (power output was ca. 5 mW). The electron paramagnetic resonance (EPR) signals were recorded at room temperature by a Bruker A300-10/12/S-LC spectrometer operating at X-band frequency (v ≈ 9.4 GHz) and 100-kHz filed modulation. Thermogravimetry and differential scanning calorimetry (TG-DSC) of the samples were conducted on a Netzch thermoanlyzer STA-449-F5 at a heating rate of 10 °C min^{-1} in a high-purity N_2 flow. X-ray diffraction (XRD) characterization were performed by a Philips X'pert Pro diffractometer. The X-ray tube was operated at 40 kV and 40 mA and the Ni-filtered Cu Kα radiation (λ = 0.15418 nm) is employed. The data were collected in a range of 2θ = 10–80°, and a scanning speed of 10° min^{-1} with a interval of 0.02° was set. X-ray photoelectron spectroscopy (XPS) measurements were conducted using a PHI 5000 Versa Probe system with a monochromatic Al Kα radiation (1486.6 eV, 15 kW). All binding energies were calibrated by the adventitious C1 s (284.6 eV) to compensate for surface charge effects.

Hydrogen temperature programmed reduction (H_2-TPR) analysis was carried out using 7 vol.% H_2/Ar mixture as reducing agent, and oxygen temperature-programmed desorption (O_2-TPD) analysis was performed using pure oxygen. The sample (100 mg) was pretreated at 200 °C for 1 h in a N_2 stream firstly, and then the 7 vol.% H_2/Ar mixture stream or a pure oxygen stream was introduced and the temperature raised from 50 °C to 900 °C. Both the H_2-TPR and O_2-TPD data were collected on a Pantech Instruments Finesorb-3010 chemisorption analyzer. Ammonia temperature programmed desorption (NH_3-TPD, 1 vol.% NH_3/N_2) experiments were performed on a multifunction chemisorption analyzer. Approximately 100 mg of sample was pretreated by pure N_2 at 350 °C for 1 h. Then, the sample was saturated with NH_3-N_2 mixture at room temperature for 1 h and flushed by pure N_2 at 100 °C for 1 h. Finally, the temperature raised to 600 °C at a rate of 10 °C min^{-1}.

The *in situ* DRIFT spectra were collected on a Nicolet Nexus 5700 FTIR spectrometer with a scanning number of 32 at a resolution of 4 cm^{-1}, and a diffuse reflectance reaction cell (HARRICK) was used. The sample was pretreated in a flowing N_2 stream at 400 °C for 1 h and the sample background was collected at various target temperature during the cooling process. For the experiments of NH_3 or NO + O_2 adsorption–desorption, the reaction cell with sample was saturated with NH_3-N_2 (1% NH_3 by volume) or NO-N_2 + O_2-N_2 (500 ppm NO and 5% O_2 by volume) for 1 h at room temperature, then the sample is purged by N_2 for 20 min and the spectra were recorded at target temperature by raising the temperature from 50 °C to 400 °C. For co-adsorption of NH_3 + O_2 + NO, the spectra were collected under the stream of NH_3-N_2 + NO-N_2 + O_2-N_2 ([NH_3] = [NO] = 500 ppm, 1 h for adsorption saturated and recorded at different desired temperatures from 100 to 400 °C).

The Vienna ab initio simulation package (VASP) was employed to perform the Spin-polarized period DFT calculations of Sm-doped CeO_2 (111), and the projector-augmented wave (PAW) potentials were used during the calculation [31–33]. The Kohn-Sham equations was solved by the generalized gradient approximation (GGA) with Perdew-Burke-Ernzerh (PBE) [34]. The f-orbitals of Ce and Sm atoms are Hubbard corrected with U = 8 eV. A cutoff energy of 400 eV is used for the plane wave basis of valence electron wave function. A minimum of 4 × 4 × 4 k-points was sampled for the bulk calculations.

2.3. Activity test of catalysts

The activity of the catalysts was tested on a fixed bed, and a flowing gas with a space velocity of 90,000 h^{-1} was used. The constituent of the gas was 500 ppm NH_3, 500 ppm NO, 5 vol.% O_2, N_2, 200 ppm SO_2 (when used) and 5 vol.% H_2O (when used). Thermo Fisher IS10 FTIR spectrometer was employed to detect the concentrations of NO, NH_3, N_2O and NO_2 gases. The activity data were recorded at every target temperature after stabilizing for 60 min. The NO conversion and N_2 selectivity rate of the reaction were calculated by the formulas as follows:

$$\text{NO covversion (\%)} = \frac{[NO]_{in} - [No]_{out}}{[NO]_{in}} \times 100\%$$

$$N_2\,\text{selectivity(\%)} = \frac{[NO]_{in} - [NO]_{out} + [NH_3]_{in} - [NH_3]_{out} - [NO_2]_{out} - 2[N_2O]_{out}}{[NO]_{in} - [NO]_{out} + [NH_3]_{in} - [NH_3]_{out}}$$

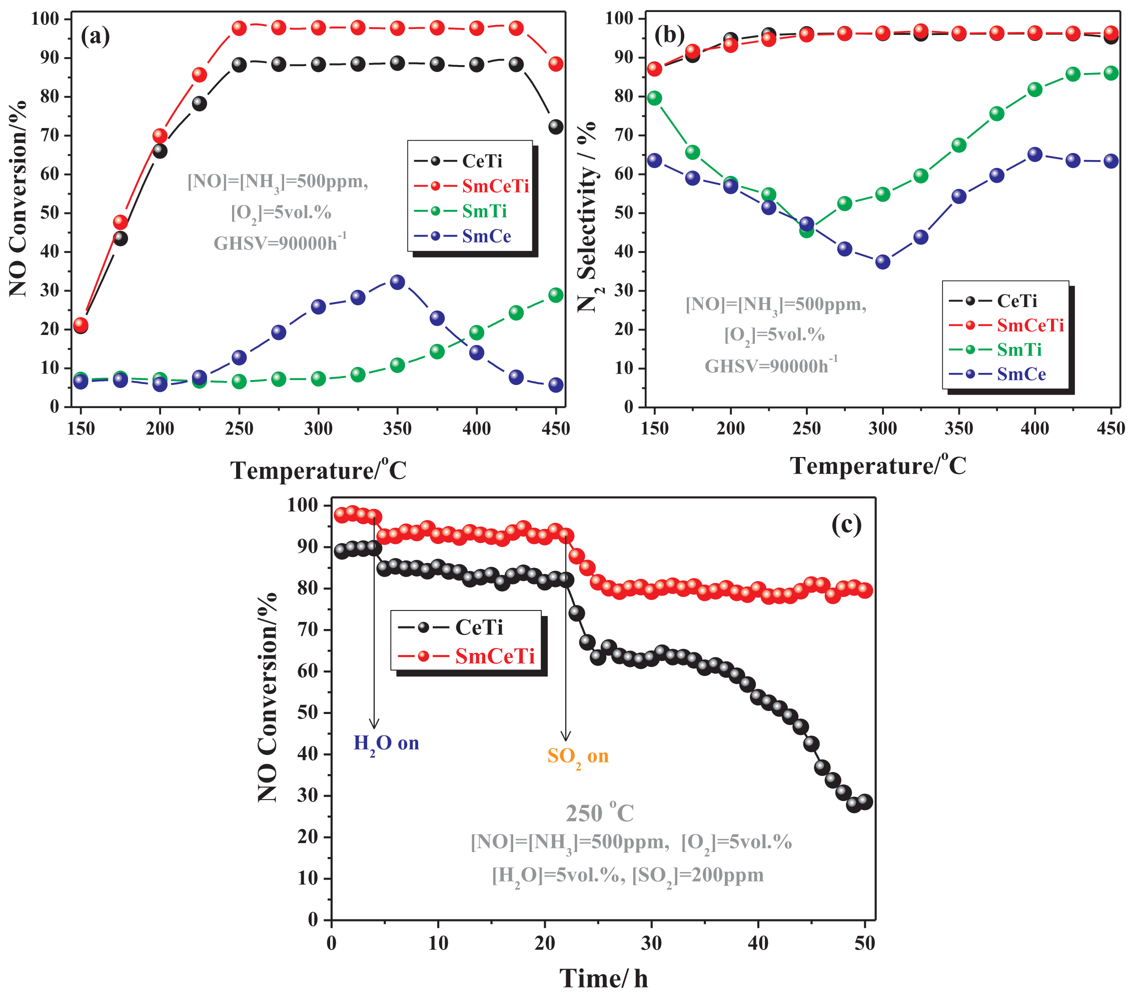

Fig. 1. NO conversion (a) and N_2 selectivity (b) of samples in NH_3-SCR as a function of temperature. 5 vol.% H_2O and 200 ppm SO_2 tolerance tests (c) at 250 °C over CeTi and SmCeTi samples.

3. Results and discussion

3.1. Catalytic activity, SO_2 or/and H_2O tolerance properties

In the CeTi catalyst, the ratio of the Ce/Ti is fixed at 0.3 for the highest activity of it among the CeO_2-TiO_2 catalysts with different ratios [24]. The activities of SmCeTi catalysts with different ratios of Sm/Ce are studied, and the results are displayed in **Fig. S1** (*Supporting Information*). As can be seen, $Sm_{0.1}Ce_{0.3}Ti$ catalyst exhibits the best activity among different Sm doped CeTi catalysts in a wide operating temperature window. Consequently, the $Sm_{0.1}Ce_{0.3}Ti$ (hereafter denoted as SmCeTi) is selected as the target catalyst for further study.

Fig. 1**(a)** and **(b)** show the results of NO conversion and N_2 selectivity of the NH_3-SCR reaction on the SmCe, SmTi, CeTi and SmCeTi catalysts. For SmCe and SmTi samples, both of them exhibit low NO conversion and N_2 selectivity from 150 °C to 450 °C, with the maximum NO conversion only ~28% and ~32%, respectively. While the CeTi catalyst is shown to exhibit a relative high catalytic activity, over which ~66% NO conversion is achieved at 200 °C and ~89% NO conversion is reached at 250 °C. After Sm species are introduced into CeTi catalyst, the activity of SmCeTi is close to that of CeTi below 200 °C. However, the SmCeTi catalyst shows high catalytic activity at temperatures higher than 200 °C. Furthermore, the ~98% NO conversion is achieved at 250 °C. In addition, the N_2 selectivity of the CeTi and SmCeTi catalysts are both high, and over 96% N_2 selectivity are attained in the whole test temperature range.

In practical working conditions, SO_2 and H_2O are both the main components in exhaust gases of coal-fired power plants, and the resistance ability to SO_2 and H_2O are important for evaluating NH_3-SCR catalysts [35]. The influence of SO_2 or/and H_2O on catalytic performance of CeTi and SmCeTi catalysts are investigated at 250 °C. **Fig. S2** shows the catalytic activity of the CeTi and SmCeTi catalysts when the 200 ppm SO_2 presents. For CeTi catalyst, the NO conversion decreases gradually to ~60% during the entire test time. While the NO conversion of SmCeTi catalyst maintains at ~88% finally. The influences of H_2O and SO_2 on CeTi and SmCeTi catalysts are evaluated, and the results are shown in Fig. 1**(c)**. When 5 vol.% vapor is introduced into the feed gas, the NO conversions of CeTi and SmCeTi is dropped by ~5%, possibly due to the competitive adsorption of H_2O with NO/NH_3 on the active sites [35]. In the next 18 h, the NO conversions of two samples are almost unchanged, which indicates that H_2O can not result in obvious deactivation of catalysts at 250 °C. When 200 ppm of SO_2 is simultaneously introduced into the feed gas with 5% H_2O, the NO conversion gradually decreases from ~82% to ~27% for CeTi catalyst. However, the SmCeTi catalyst exhibits significant performance for SO_2 and H_2O resistance, and the NO conversion remains at ~80%. In summary, the introduction of samarium species into CeTi mixed oxide catalysts significantly improves the activity and tolerance of H_2O and SO_2 for NH_3-SCR reaction.

3.2. Composition and textural properties (ICP, BET, XRD, Raman and EPR) of catalysts

The ICP-OES results suggest that the molar ratios of different metal

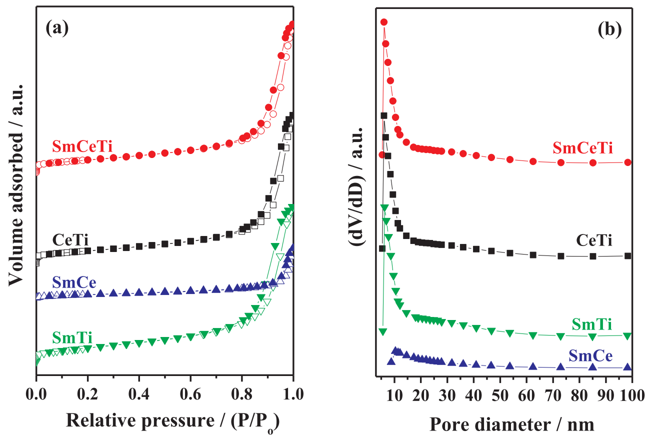

Fig. 2. The N_2 adsorption-desorption isotherms (a) and BJH pore distribution curves (b) of SmTi, SmCe, CeTi and SmCeTi samples.

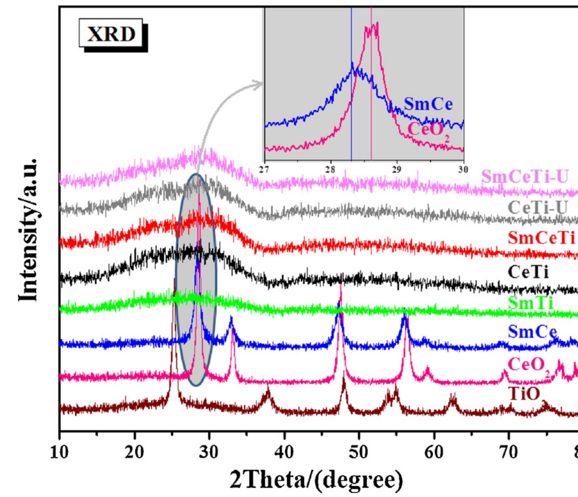

Fig. 3. XRD patterns of TiO_2, CeO_2, SmCe, SmTi, CeTi, SmCeTi, CeTi-U and SmCeTi-U.

Table 1
The surface area of fresh and used samples.

Catalysts	Fresh sample S_1 ($m^2\,g^{-1}$)	Used sample S_2 ($m^2\,g^{-1}$)	$\Delta S = \frac{S_1 - S_2}{S_1}$(%)
CeTi	201	149	25.9%
SmCeTi	257	229	10.9%

elements in the prepared catalysts are very close to the initial feed ratios (**Table S1**). Fig. 2 displays N_2 adsorption-desorption isothermals and the corresponding BJH pore size distribution curves of SmTi, SmCe, CeTi and SmCeTi catalysts. As shown in Fig. 2**(a)**, the isotherms of all catalysts are of representative type IV and a well-defined H2-type hysteresis loops as judged by IUPAC, which is the feature of mesoporous materials due to the texture of interparticle mesoporosity [19,36]. In Fig. 2**(b)**, the pore size distribution curves of these samples determined by the BJH method show one single narrow peak centered at 14.5–17.1 nm, suggesting that these samples possess relative uniform mesopore size distributions. The textural data of SmTi, SmCe, CeTi, SmCeTi samples are listed in **Table S2** and the catalysts used after NH_3-SCR (including SO_2 and H_2O) reaction (denoted as CeTi-U and SmCeTi-U) are displayed in Table 1. As can be seen, the specific surface area, pore volume, and average pore diameter decrease in the order of SmCeTi > SmTi > CeTi > SmCe. In addition, it should be noted that the specific surface area of used catalysts obviously decrease compared with the fresh catalysts, which should be ascribed to the sulfate species cover on the surface of catalysts after the NH_3-SCR reaction. The descent rate (ΔS) of the surface area of CeTi-U(25.9%) is greater than that of SmCeTi-U (10.9%), which implies that Sm species introducing into CeTi is beneficial to preventing the surface sulfation of catalysts.

Fig. 3 shows XRD patterns of TiO_2, CeO_2, SmCe, SmTi, CeTi, and SmCeTi samples, and the patterns of CeTi-U and SmCeTi-U catalysts are also included. Pure TiO_2 presents as anatase (PDF ICDD 84–1286), and the CeO_2 and SmCe present as cerianite (PDF ICDD 34-0394). No diffraction peaks of Sm_2O_3 can be observed in SmCe sample. Furthermore, it should be noted from the inset in Fig. 3 that doping of Sm to CeO_2 leads the shifting of diffraction peaks towards lower angle direction. According to the Bragg's Law, the shifting of diffraction peaks should be ascribed to the incorporation of Sm into the CeO_2 lattice, which is due to the larger ionic radii of Sm^{3+} (0.108 nm) than the Ce^{4+} (0.097 nm). The results of Raman spectra (CeO_2 and SmCe) are shown in **Fig. S3.** The F_{2g} band of SmCe sample shifts to the lower wavenumber compared with that of CeO_2, and no bands of Sm_2O_3 (generally observed at ~375 cm^{-1}) are found in the Raman spectra of SmCe sample [37]. The XRD and Raman spectra suggest the incorporation of Sm into the CeO_2 lattice. Moreover, no obvious peak can be observed for SmTi, CeTi and SmCeTi revealing a amorphous structure of them, which may maximize the interaction among different species (Sm, Ce and Ti) [24,38]. For the used catalysts, there is no obvious change for the diffraction patterns of the two samples compared with the fresh samples. The results suggest that the structure of catalysts are unchanged and no crystalline sulfate species form on the surface of catalysts during the NH_3-SCR reaction.

Raman analysis is also performed to detect the oxygen vacancies of the samples, and the results are displayed in Fig. 4**(a)**. For SmTi, the faint peak near 144 cm^{-1} is assigned to B_{1g} mode of anatase-TiO_2 [2,3]. SmCe sample exhibits a prominent peak centered at 467 cm^{-1}, which indicates the F_{2g} mode of fluorite cubic structure CeO_2 [22,39]. The peaks at 279 and 604 cm^{-1} are assigned to oxygen vacancies due to the existence of Ce^{3+} [20,39]. For the CeTi and SmCeTi catalysts, the weak peaks located at around 140 and 467 cm^{-1} are assigned to the B_{1g} mode of TiO_2 and F_{2g} mode of CeO_2, respectively. The peaks around 279 and 604 cm^{-1} are related to oxygen vacancies which can improve oxygen storage and increase the transformation frequency between Ce^{3+} and Ce^{4+} [20]. In addition, the peaks intensities of the SmCeTi catalyst are higher than that of CeTi, indicating that more oxygen vacancies exist in the SmCeTi catalyst. More oxygen vacancies will facilitate the NO oxidation, and further promotes the NH_3-SCR reaction [40]. EPR analysis is employed to further confirm the existence of oxygen vacancies (Fig. 4**(b)**). As can be seen, for SmTi, CeTi and SmCeTi samples, the Sm or/and Ce doping into TiO_2 significantly produce the oxygen vacancies (g = 2.002) [26]. The signal for oxygen vacancies of SmCe sample is weaker than that of the Ti including samples. The results suggest Sm or Ce doping into TiO_2 will produce more oxygen vacancies than that of Sm doping into CeO_2, which may be due to the larger radius differences between Sm/Ce and Ti atoms.

3.3. Surface constituent and chemical states (XPS) of catalysts

Fig. 5 displays the XPS spectra of Ti 2p, Ce 3d, Sm 3d, O 1 s and S 2p for different samples, and the results are summarized in Table 2. As shown in Fig. 5**(a)**, the binding energies of Ti 2p are approximately located at 459.2 and 464.9 eV for all the samples, suggesting that the Ti species exhibit +4 valence state [5,14]. Fig. 5**(b)** and **(c)** display the Sm 3d and Ce 3d XPS spectral results. The Sm 3d spectra of the samples can be fitted to two peaks for all samples, the peaks at ~ 1083.2 eV and ~ 1080.4 eV represent Sm^{3+} and Sm^{2+}, respectively [5,41]. XPS spectra of Ce 3d of all samples can be deconvoluted into eight peaks, which corresponds to four pairs of spin-orbit doublets [26,27]. The peaks marked as u (901.0 eV), u″(908.1 eV) and u‴ (916.5 eV) arise from the contribution of Ce^{4+} $3d_{3/2}$, and the peaks labeled as v

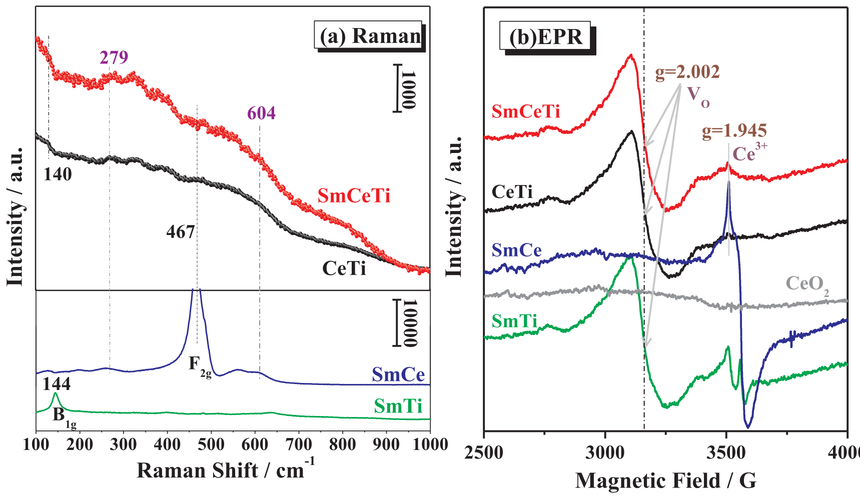

Fig. 4. Raman (a) and EPR (b) spectra of SmTi, SmCe, (CeO_2), CeTi and SmCeTi samples.

(882.4 eV), v″(888.9 eV) and v‴ (898.3 eV) arise from Ce^{4+} $3d_{5/2}$. In addition, the existence of Ce^{3+} is proved by the peaks labeled as u′(903.8 eV) and v′(885.5 eV) [2,20,26,42]. The content of surface Ce^{3+} over these samples is calculated by the equation as follows [35], and listed in Table 2.

It can be seen from Table 2 that the contents of Ce^{3+} of SmCeTi are larger than that of CeTi. Meanwhile, the contents of Sm^{3+} of SmCeTi are higher than that of SmTi. Therefore, the valence state of the Ce species is reduced, while it is increased for Sm species compared with the CeTi and SmTi catalysts, respectively. These results suggest the

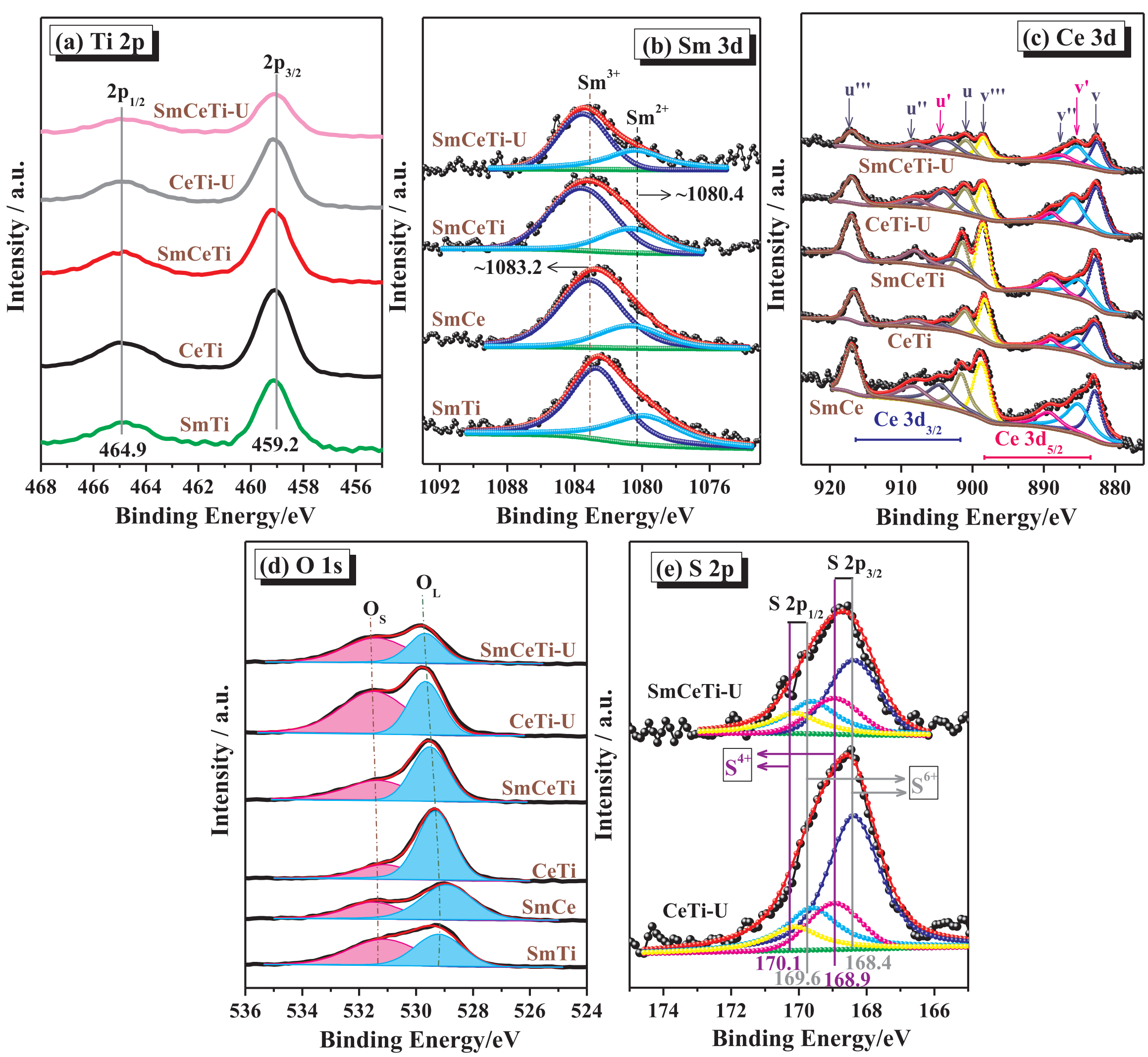

Fig. 5. XPS spectra of the obtained samples: (a) Ti 2p, (b) Sm 3d, (c) Ce 3d, (d) O1 s and (e) S 2p.

Table 2
The surface compositions of the different samples.

Samples	Sm^{3+}/Sm (%)	Ce^{3+}/Ce (%)	O_S/O (%)
SmTi	64	–	–
SmCe	75	39	–
CeTi	–	14	22
SmCeT	77	25	45
CeTi-U	–	40	63
SmCeTi-U	75	39	58

electrons can transfer from Sm to Ce in the SmCeTi catalyst, *i.e.*, $Ce^{4+} + Sm^{2+} \rightleftharpoons Ce^{3+} + Sm^{3+}$. In order to further explore the doping effect of Sm and obtain the information of electron transfer, the differential charge densities are calculated for Sm-substituted CeO_2 using the following equation:

$$\rho_{diff} = \rho_{CeSmO} - (\rho_{CeO} + \rho_{Sm})$$

As shown in Fig. 6**(c)** and **(d)**, the oxidation state of the Sm atom increases due to the lossed electrons, suggesting the electrons can transfer from Sm to Ce atoms, which is accordance with the results of XPS.

Additionally, as illustrated in Table 2, the ratios of Ce^{3+}/Ce in the CeTi-U and SmCeTi-U samples are more than that of the corresponding fresh samples, which is ascribed that SO_2 can react with Ce^{4+} species in the presence of O_2 as following reaction [35]:

$$2CeO_2 + 3SO_2 + O_2 = Ce_2(SO_4)_3$$

Interestingly, it should be noted that the growth rate of Ce^{3+} ($\Delta M = M_{Used}$- M_{Fresh}) of SmCeTi-U (14%) is lower than that of CeTi-U (26%), which represents that doping of Sm species into CeTi prevents the sulfation of surface Ce species in the SmCeTi catalyst and improves the sulfur resistance efficiency of the catalyst.

The O 1 s (Fig. 5**(d)**) peak can be fitted to two peaks referred to the lattice oxygen at lower binding energy (~529.5 eV, hereafter denoted as O_L) and the surface oxygen at higher binding energy (~531.4 eV, hereafter denoted as O_S) [3,11,39]. As shown in Table 2, the contents of O_S in the SmCeTi (45%) sample are much higher than that in the CeTi (22%) sample, suggesting that the amounts of O_S species greatly increase after the introduction of samarium, which is beneficial to the NO oxidation to NO_2 in a $NO + NH_3 + O_2$ reaction [26]. Moreover, compared with the CeTi and SmCeTi samples, more O_S species can be detected in the used samples, which should be attributed to the sulfates formed on the surface of used catalysts [35]. Meanwhile, it should be noted that the amount of O_S species in SmCeTi-U catalyst is less than that of CeTi-U catalyst, which further proves that the formation of sulfate over SmCeTi catalyst could be suppressed by the incorporation of Sm. In addition, as can seen in Fig. 5**(e)**, the S 2p spectra can be detected in the used samples. The peak at ~168.6 eV and 169.6 eV are respectively assigned to S^{6+} $2p_{3/2}$ and $2p_{1/2}$, and the peak at ~168.9 eV and 170.1 eV are attributed to S^{4+} $2p_{3/2}$ and $2p_{1/2}$, respectively [4,13,43–45]. Thus, it can be concluded that both SO_4^{2-} and SO_3^{2-} generate on the surface of catalysts in the NH_3-SCR reaction with appearance of SO_2.

3.4. Redox properties and surface acidity

The redox properties of the catalysts are closely related to the activities in the SCR reaction. Fig. 7 **(a)** displays the H_2-TPR profiles of CeTi, SmTi, SmCe and SmCeTi catalysts, and the reduction peaks are deconvoluted fitted with Gaussian-Lorentz function. The reduction temperature and amounts of H_2 consumption are displayed in Table 3. The reduction profile of SmTi, SmCe and CeTi can be fitted to two peaks (α and β) mainly related to the reduction of the surface oxygen and lattice oxygen, respectively [24,46,47]. The reduction temperatures of α and β are shown in Table 3, and the order of the temperature is SmTi > SmCe > CeTi, suggesting the CeTi catalyst shows the best reducibility among the three samples. For the SmCeTi catalyst, the reduction peak at 424 °C (α) and 506 °C (β) can also be attributed to the reduction of the surface oxygen and lattice oxygen, respectively, and the peak areas of them are higher than that of CeTi sample. In addition, the SmCeTi catalyst shows one more reduction peak at 576 °C (denoted as γ) compared with CeTi sample. As can be seen, the reduction temperature range of peaks (α and β) for the SmCe and CeTi sample are all included in the reduction temperature range of peaks (α and β) for SmCeTi. However, the reduction temperature of peak β for SmTi sample is much higher than that of the other catalysts. Combined the reduction profiles of SmTi, SmCe and CeTi samples, it seems reasonable that peak γ is ascribed to the reduction of lattice oxygen of Sm-O-Ti in the SmCeTi. Furthermore, the incorporation of Sm to the CeTi lattice induces the structure modification and enhances the diffusion of O^{2-} anions within the lattice [48]. Thus, all the reduction peaks shift to

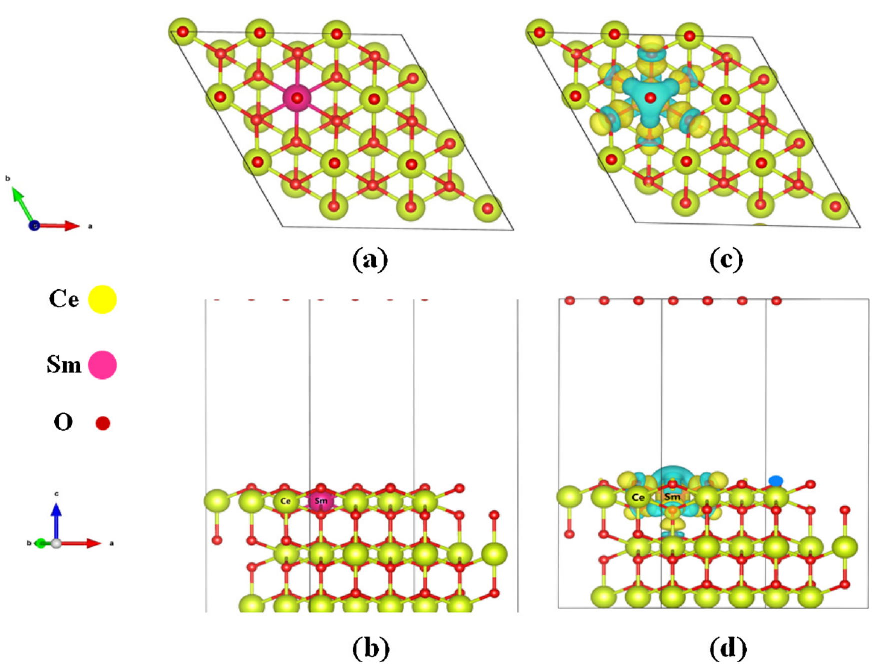

Fig. 6. Spin-polarized period DFT calculations for the Sm-doped CeO_2 (111) model: (a) top view and (b) side view. Differential charge densities of Sm-substituted CeO_2 (111): (c) top view and (d) side view. The blue color indicates the loss of electrons (For interpretation of the references to colour in this figure legend, the reader is referred to the web version of this article).

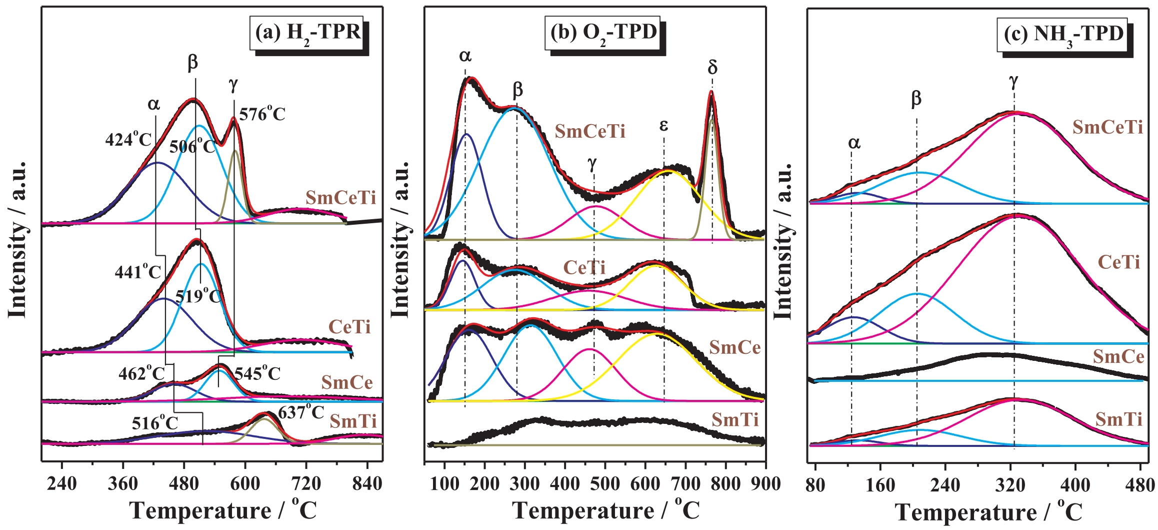

Fig. 7. H_2-TPR (a) O_2-TPD (b) and NH_3-TPD (c) curves of SmTi, SmCe, CeTi and SmCeTi samples.

Table 3
The temperature of reduction peaks and actual H_2 consumption of the samples.

Samples	Reduction temperature/°C			Actual H_2 consumption (μmol/g)
	Peak α	Peak β	Peak γ	
SmTi	516	–	637	–
SmCe	462	545	–	–
CeTi	441	519	–	153
SmCeTi	424	506	576	224

lower temperature with the incorporation of Sm to the CeTi lattice, which is beneficial for catalytic activity of the NH_3-SCR reaction. In addition, the amounts of H_2 consumption (~224 μmol/g) of SmCeTi catalyst is also much higher than that of CeTi catalyst (~153 μmol/g). Above results suggest that the reducibility of CeTi catalysts is promoted by the addition of Sm species.

The O_2-TPD profiles are shown in Fig. 7 **(b)**. For SmCe and CeTi catalysts, there are four O_2 desorption peaks (denoted as α, β, γ and ε, respectively) in the temperature range of 50–900 °C. The α peak (~149 °C) corresponds to the surface chemical adsorbed oxygen [36,49]. The β (~281 °C) and γ (~473 °C) peaks can be respectively assigned to the desorption of chemically adsorbed $O_{2(ad)}^{-}$ and $O_{(ad)}^{-}$ species, which is related to the surface oxygen defects [49]. Additionally, the ε peak at 646 °C is ascribed to the desorption of surface lattice oxygen [17,36]. The desorption peaks of SmTi sample are very weak suggesting the poor oxygen storage capacity of the SmTi sample. The desorption profiles of SmCeTi catalyst is similar to that of CeTi, and α, β, γ and ε peaks can be observed. However, one high-temperature desorption peak at 767 °C (denoted as *δ*) appears, which can not be detected in SmCe and SmTi samples. It has been reported that the incorporation of Sm to the CeTi lattice enhances the diffusion of O^{2-} anions within the lattice, accordingly, the *δ* peak may be attributed to the unstable lattice oxygen produced by Sm doping [16]. It can be clearly observed that the peak area of SmCeTi is much larger than that of CeTi, suggesting that the OSC of SmCeTi catalyst is greater than that CeTi catalyst, which is significantly improved by Sm species addition.

NH_3-TPD is performed to investigate the surface acidity of the catalysts, and the results are shown in Fig. 7**(c)**. NH_3 desorption can be detected in a wide temperature range due to the different stabilities of adsorbed NH_3 species on different acidic sites. The α peak around 125 °C are assigned to the physical adsorbed NH_3. The β (~204 °C) and γ (~324 °C) peaks can be assigned to the chemical adsorbed NH_3 at weak and strong acid sites, respectively [5,16,20]. As seen from the areas of total and each fitted peak, the SmCe sample shows the lowest peak areas, *i.e.*, the fewest acid sites. In addition, after the quantification of the NH_3 adsorption amount (based on peak area, as shown in **Table S3**), it can be known that only some strong acid sites exist and there are nearly no weak acid sites. The amounts of acid sites on SmTi sample are higher than that in SmCe sample, including weak acid sites and strong acid sites. Furthermore, the amounts of acid sites on CeTi sample are obviously higher than that of SmTi sample, suggesting the interaction of Ce and Ti producing large amounts of acid sites. The total NH_3 adsorption amounts decrease by Sm doping. Thus, it can be concluded that doping of samarium to CeTi catalyst leads to a reduction of the surface acidity of the catalyst. It is a universal acknowlegement that the NH_3-SCR catalysts exhibit the best activity when the acidity and redox property achieve an appropriate balance [50–52]. The decrease of surface acidity may be helpful for the balance of acidity and redox property of SmCeTi catalyst, which induces the better activity.

3.5. In situ DRIFT studying the adsorption properties of NH_3, NO + O_2 and NO + O_2+NH_3 on the catalyst surfaces

3.5.1. The NH_3-adsorption in situ DRIFTS on the catalysts

The NH_3-adsorption *in situ* DRIFTS spectra on the CeTi and SmCeTi catalysts as a function of temperature are displayed in Fig. 8. For CeTi catalysts (Fig. 8 **(a)**), several peaks in the range of 1800-1100 cm^{-1} and 3400-3100 cm^{-1} are detected. The peaks at 1665 and 1451 cm^{-1} are attributed to ionic NH_4^+ bound to Brønsted acid sites, while the peaks at 1597 and 1166 cm^{-1} are ascribed to coordinated NH_3 bound to Lewis acid sites [8,17,21,23,53]. In the high wavenumber range, N—H stretching vibration modes of the coordinated NH_3 at 3371, 3246 and 3148 cm^{-1} are observed [21,26]. All peaks became weaker with the temperature increasing from 50 to 400 °C. With the increase of temperature, the symmetric N—H bending vibration of the coordinated NH_3 groups shifts from 1166 cm^{-1} to 1190 cm^{-1} This blueshift is attributed to the broken of hydrogen bonds between the chemisorbed NH_3 groups [54]. The peaks intensities of NH_3 adsorbed on Brønsted acid sites (1665 and 1451 cm^{-1}) decrease distinctly at higher temperature and nearly disappear at approximately 300 °C due to the desorption or/and decomposition of ionic NH_4^+. In contrast, the peaks representing NH_3 adsorbed on Lewis acid sites (1597 and 1190 cm^{-1}) remain even at 400 °C, which indicate that the strength of Brønsted acid sites are weaker than that of the Lewis acid sites on the CeTi catalyst surface. Considering the NH_3-TPD results, the weak and strong acid sites should be corresponding to the Brønsted and Lewis acid sites, respectively.

For the surface of the SmCeTi catalyst, ionic NH_4^+ (1669 cm^{-1} and

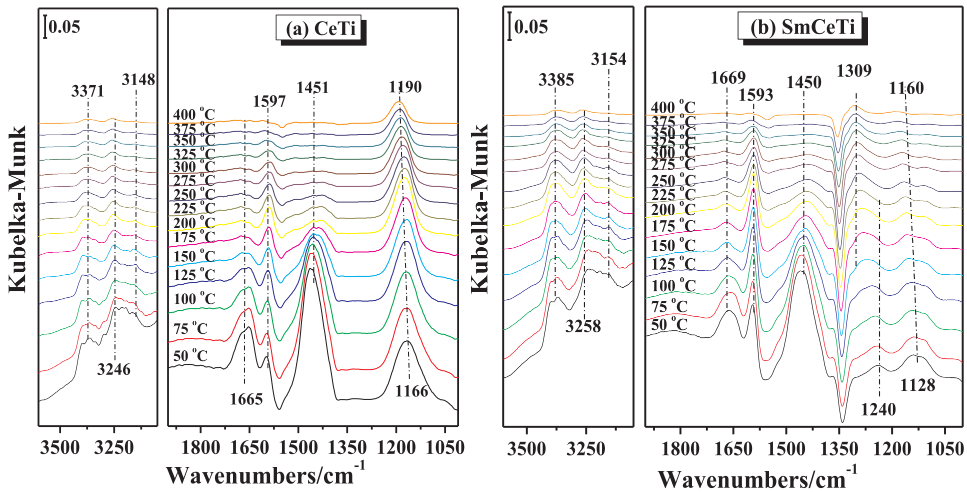

Fig. 8. *In situ* DRIFTS spectra of NH_3 adsorption–desorption over the CeTi (a) and SmCeTi (b) catalysts from 50 to 400 °C with a temperature interval of 25 °C.

1450 cm^{-1}), coordinated NH_3 (1593 cm^{-1} and 1192 cm^{-1}) are also discovered, as shown in Fig. 8 **(b)**. In the high wavenumber range, N—H stretching vibration modes of the coordinated NH_3 at 3385, 3258 and 3154 cm^{-1} are also observed. Compared with CeTi catalyst, there is a considerable difference in SmCeTi catalyst. A new peak is detected at 1309 cm^{-1} started from 125 °C, which is ascribed to amide species (NH_2) [17,35]. The XPS results suggest that decoration of samarium to CeTi catalyst induces the facile switch between Ce^{4+} and Ce^{3+} species, which is in favor of the adsorption and activation of NH_3 species producing NH_2 [55]. The NH_2 groups can react with NO as Eq. (1), and promotes the proceeding of NH_3-SCR reaction [17,55].

$$NH_2 + NO \rightarrow NH_2NO \rightarrow N_2 + H_2O \quad (1)$$

3.5.2. The NO + O_2 adsorption in situ DRIFTS of catalysts

Fig. 9**(a)** shows the NO + O_2 adsorption *in situ* DRIFTS spectra on CeTi catalyst at different temperatures. Six peaks at 1634, 1600, 1525, 1453, 1281 and 1225 cm^{-1} are detected at 50 °C, which can be assigned to adsorbed NO_2, bidentate nitrate, monodentate nitrate, linear nitrite, monodentate nitrate and bridging nitrate, respectively [3,10,16,21,29]. With temperature increasing, the changes of the peaks intensities for different NO_x species are different. The areas of peaks as a function of temperature are shown in Fig. 9**(b)**. As can be seen, the peak intensities of monodentate nitrate, linear nitrite and bridging nitrate all decrease with the temperature increasing from 50 to 400 °C. While the peak intensity of adsorbed NO_2 species increases with the temperature increasing. which suggests that the monodentate nitrate, linear nitrite and bridging nitrate species may transform to NO_2 species on the CeTi catalyst surface. In addition, the bidentate nitrate is relative stable on the surface of catalyst.

Fig. 9**(c)** presents the *in situ* DRIFTS spectra of NO + O_2 adsorption-desorption on SmCeTi catalyst, which are very similar to that of CeTi catalyst. The adsorbed NO_2 (1634 cm^{-1}), bidentate nitrate (1600 cm^{-1}), monodentate nitrate (1525 and 1284 cm^{-1}), linear nitrite (1455 cm^{-1}) and bridging nitrate (1231 cm^{-1}) can be observed. Interestingly, it can be found in Fig. 9**(d)** that the peak intensities of the adsorbed nitrate/nitrite species on the SmCeTi catalyst surface are stronger than those on the surface of CeTi catalysts, suggesting that the doping of Sm into the CeTi can improve the adsorption ability of nitrate/nitrite species efficiently, which can improve the catalytic activity of the NH_3-SCR [17,26]. Combined the results reported previously and our XPS characterization [38,56,57], the increase of nitrate/nitrite species over the surface of SmCeTi catalyst may be attributed to the formation of the redox couples Sm^{3+}/Sm^{2+} and Ce^{4+}/Ce^{3+}, in which electrons may transfer between them through the "Sm–O–Ce" bridge structure. Similar to the Cr-Mn and Sm-Mn system [5,12], O_2 can get electron from Ce^{3+} producing O- and Ce^{4+}, and NO give electron to Sm^{3+} producing NO^+ and Sm^{2+} during the NH_3-SCR reaction. Finally, the electron transfers from Sm^{2+} to Ce^{4+}, and a redox cycle forms in this process, as shown in Scheme 1. The nitrate species can be generated continuously *via* the Sm^{3+}/Sm^{2+} and Ce^{4+}/Ce^{3+} redox couples as the following reaction:

$$O_2 + 2Ce^{3+} \rightarrow 2O_{ad}^{-} + 2Ce^{4+} \quad (2)$$

$$NO + Sm^{3+} \rightarrow Sm^{2+} + NO_{ad}^{+} \quad (3)$$

$$NO_{ad}^{+} + 2O_{ad}^{-} \rightarrow NO_{3}\text{-}_{ad} \quad (4)$$

In addition, through comparing Fig. 9**(b)** and **(d)**, it can be found that the peak intensity of nitrate species over the SmCeTi catalyst surface gets weak sharply compared with that of the CeTi catalyst as the temperature increasing. This phenomenon suggests that the Sm species doped into CeTi catalyst can accelerate the decomposition/transformation of the adsorbed nitrate species.

3.5.3. In situ DRIFTS studying of the reaction between NO + O_2/NH_3 and adsorbed NH_3/NO + O_2 species over CeTi and SmCeTi catalysts

The catalysts were first purged with NH_3 for 1 h followed by N_2 purging. NO + O_2 was then introduced into the IR cell at 200 °C, and the spectra were recorded as a function of time, as shown in Fig. 10**(a)** and **(b)**. The coordinated NH_3 (3400-3100, 1597 and 1169 cm^{-1}) and ionic NH_4^+ (1665 and 1451 cm^{-1}) can be detected on the CeTi catalyst surface (Fig. 10**(a)**). After NO + O_2 was introduced to the cell, the coordinated NH_3 and ionic NH_4^+ were rapidly consumed and nearly disappear after 5 min, which suggests that coordinated NH_3 and ionic NH_4^+ can be oxidized by NO_x in the SCR reaction. The absorbed NO_x species can be observed on the catalyst surface after the pre-adsorbed NH_3 species was completely consumed, and the peaks of NO_x species including adsorbed NO_2 (1634 cm^{-1}), bidentate nitrate (1600 cm^{-1}), monodentate nitrate (1525, 1281 cm^{-1}) and bridging nitrate (1230 cm^{-1}) appear. The *in situ* DRIFTs of NO + O_2 adsorption after pre-adsorption of NH_3 was also collected for the SmCeTi catalyst, as shown in Fig. 10**(b)**. The adsorption behavior of NH_3 on the SmCeTi catalyst are similar to that on CeTi catalyst, and the coordinated NH_3 (3400-3100, 1593 and 1169 cm^{-1}), ionic NH_4^+ (1669 and 1450 cm^{-1}) and NH_2 (1309 cm^{-1}) can be observed. The absorbed NH_3 disappeared completely after 5 min when NO + O_2 were introduced, which suggested the absorbed NH_3 species bounded to both Brønsted and Lewis acidic sites on the SmCeTi surface also played the roles of reducing agents in the SCR reaction. The above results indicate that the NH_3-SCR reaction can proceed obey the Eley-Rideal (E–R) mechanism on the

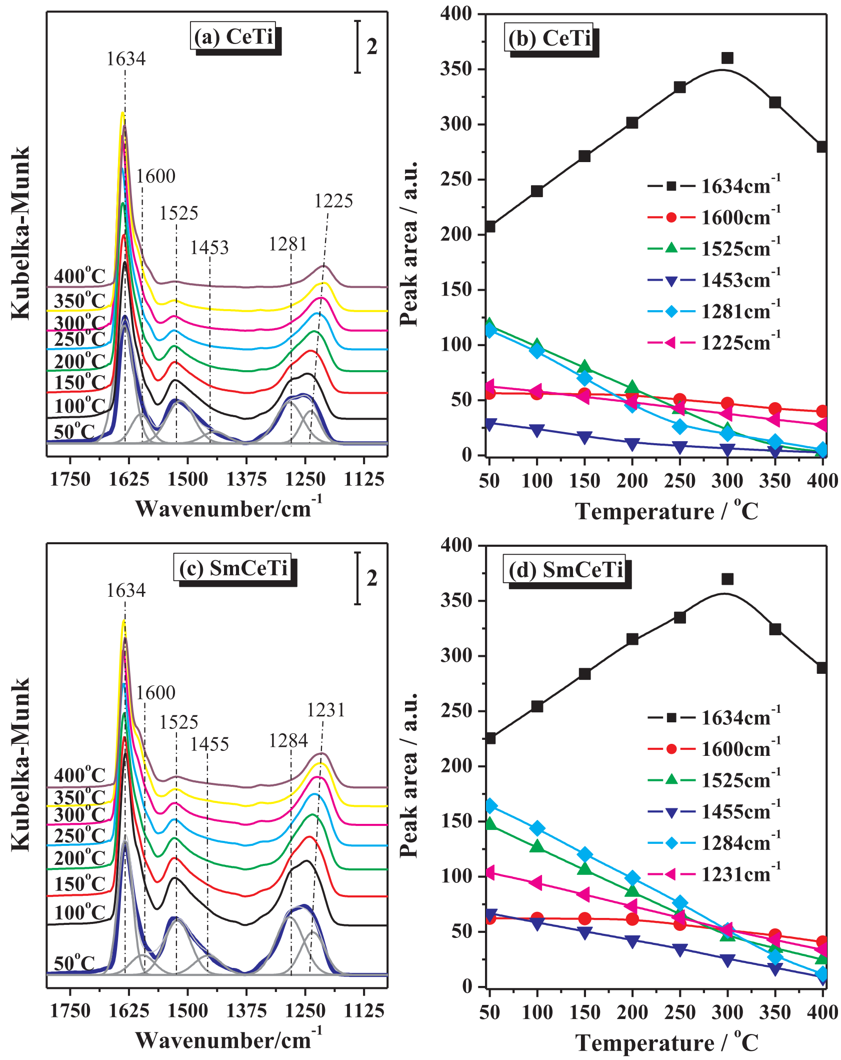

Fig. 9. NO + O_2 adsorption *in situ* DRIFTS spectra and peak areas of the adsorbed nitrate species over CeTi (a), (b) and SmCeTi (c),(d) as a function of temperature.

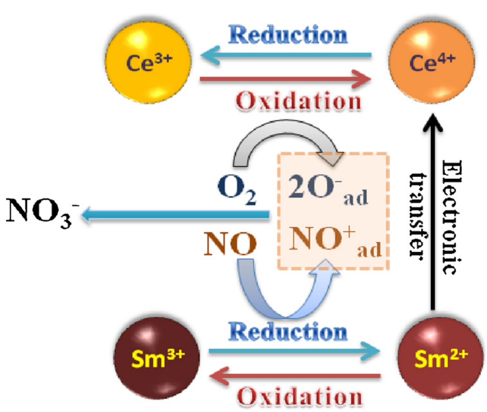

Scheme 1. Redox catalytic cycle of the low-temperature SCR reaction over the SmCeTi catalyst.

CeTi and SmCeTi catalysts surface, which are similar with the NH_3-SCR reaction catalyzed by some other catalysts, such as CeWTi [55], Cu/TiNb [3] and CuCeZr [18].

The *in situ* DRIFTs experiment of the reaction between NH_3 and pre-adsorbed NO_x species on the surface of CeTi and SmCeTi catalysts are also conducted at 200 °C for comparison, and the results are shown in Fig. 10**(c)** and **(d)**. For the CeTi catalyst (Fig. 10**(c)**), the catalyst surface is mainly covered by five kinds of nitrate species, *e.g.*, NO_2 (1634 cm^{-1}), bidentate nitrate (1600 cm^{-1}), monodentate nitrate (1525, 1281 cm^{-1}), linear nitrite (1453 cm^{-1}) and bridging nitrate (1225 cm^{-1}). The introduction of NH_3 results in disappearance of NO_2 after 10 min implying the reaction between NH_3 and NO_2. The bidentate nitrate species (1600 cm^{-1})still exists on the catalyst surface even after 50 min, suggesting that the bidentate nitrate is inactive in the SCR reaction. Similar phenomenon was also observed over the surface of MnO_x-TiO_2 [10,58] and Mn − Fe Spinel [6] catalysts. The peaks for monodentate nitrate at 1525 and 1270 cm^{-1} increase obviously with the time increasing, which may be due to two reasons. First, one adsorption site of bridging nitrate is snatched by NH_3, and then bridging nitrates transform to monodentate nitrates [22]. It can be observed that the bridging nitrates disappear as the monodentate nitrates increasing significantly after the NH_3 was injected for 10 min. Second, the NH_3 might be oxidized on the surface of catalyst forming nitrate species [55]. The NH_3 species adsorbed on the catalyst surface simultaneously, coordinated NH_3 (3400-3100, 1588, 1186 cm^{-1}) and ionic NH_4^+ (1451 cm^{-1}) can be observed. The results suggest that adsorbed NH_3 and nitrate species can coexist on the CeTi catalyst surface. The SmCeTi catalyst shows nearly the same variation with the CeTi catalyst (Fig. 10**(d)**). Moreover, NO_2 are consumed more rapidly (5 min) on the surface of SmCeTi catalyst compared to CeTi catalyst, which may be responsible for the good activity of SmCeTi catalyst. Above results suggest that the reaction between NH_3 and nitrate species are difficult

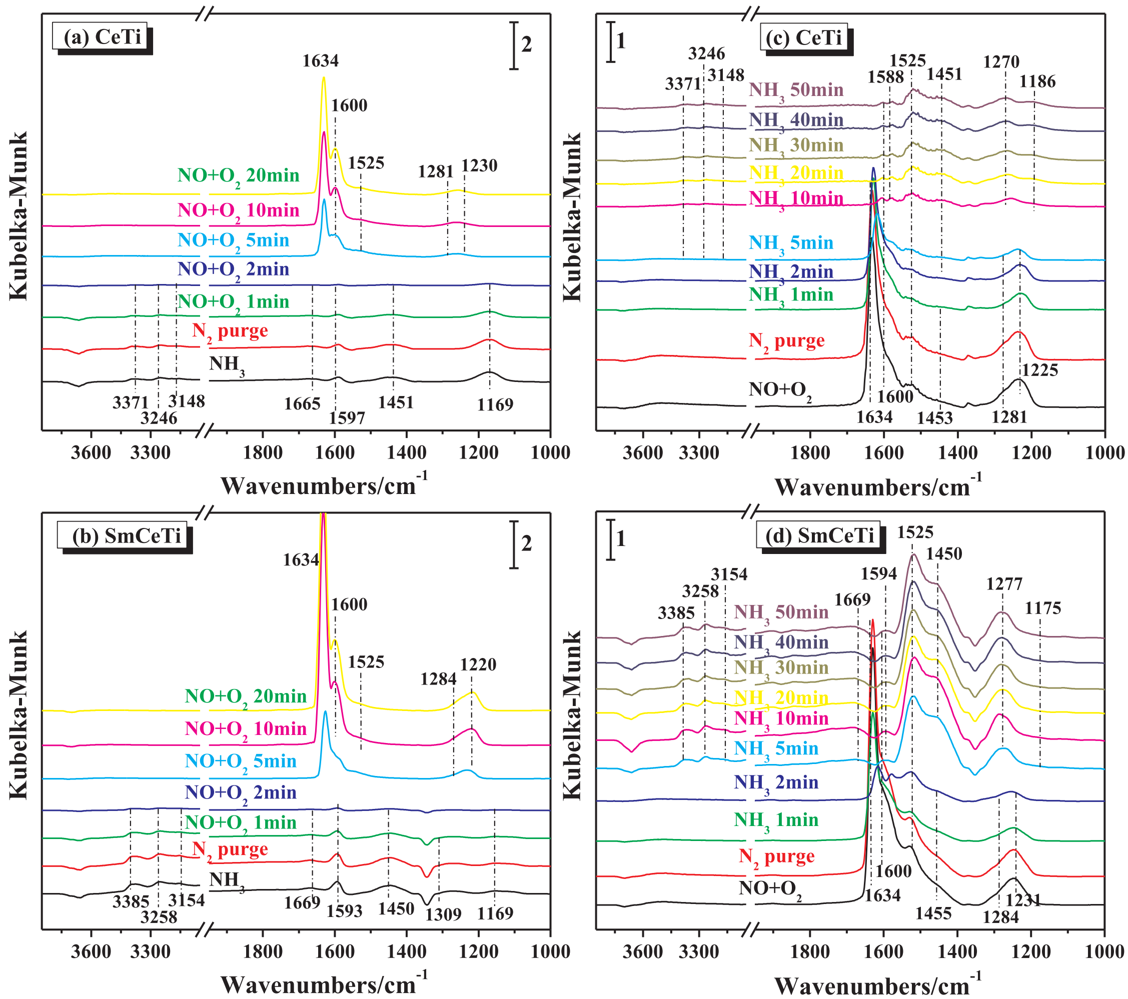

Fig. 10. DRIFT spectra taken at 200 °C of passing NO + O_2 over the NH_3 pre-absorbed on (a) CeTi and (b) SmCeTi and passing NH_3 over the NO + O_2 pre-absorbed on (c) CeTi and (d) SmCeTi for different times.

to occur, except for the reaction between NO_2 and NH_3. The experiment of the reaction between NH_3 and pre-adsorbed NO_x species further suggest that the NH_3-SCR reaction on the CeTi and SmCeTi catalysts may be largely dominated by the E-R mechanism.

3.5.4. *In situ DRIFTS studying of NH_3 + NO + O_2 reaction on the catalysts*

A flow of NO + NH_3 + O_2 gas was introduced into the reaction cell, and the surface adsorbed species were detected by *in situ* DRIFTS spectra under the reactive condition from 100 to 400 °C. Many different species, such as coordinated NH_3 on Lewis acid sites (3400-3100 cm^{-1}, 1200 cm^{-1}) [21], ionic NH_4^+ on Brønsted acid sites (1670 cm^{-1}, 1455 cm^{-1}) [55], adsorbed NO_2 (1637 cm^{-1}) [26], bidentate nitrate (1600 cm^{-1}) [55], monodentate nitrate (1525 cm^{-1}) [55] and NH_4NO_3 species (1300 cm^{-1}) [5,17,53] can be observed on CeTi at 100 °C, as shown in Fig. 11**(a)**. Compared with the spectra of single NH_3 adsorption (Fig. 8**(a)**), the peak at 1445 cm^{-1} shows stronger intensity indicating the enhanced amounts of Brønsted acidic sites on the surface of CeTi, which might be caused by the generation of water in NH_3-SCR reaction. In contrast, the adsorbed NH_3 species on Lewis acid sites is very weak, suggesting some Lewis acid sites have converted to the Brønsted acidic sites. The increase of temperature results in a decrease of peaks intensities of the coordinated NH_3, ionic NH_4^+, adsorbed NO_2, monodentate nitrate and NH_4NO_3 species, suggesting these species are unstable with the temperature increasing. Among them, it should be noted that the peak intensity of NO_2 species are much weaker compared with that in the single NO adsorption spectra, suggesting the NO_2 is easy to be consumed in the NH_3-SCR reaction [17,21]. On the contrary, the bidentate nitrate species are firmly adsorbed on the CeTi catalyst surface, and the intensity of the peak becomes stronger with the increase of temperature. The results indicate that bidentate nitrate species are not the active species in the reaction, and they will be aggregation on the catalyst surface with the proceeding of the reaction.

Fig. 11**(b)** shows the *in situ* DRIFT spectra of NO + NH_3 + O_2 reaction on SmCeTi catalyst. There are mainly coordinated NH_3 (3400-3100 cm^{-1}, 1200 cm^{-1}), ionic NH_4^+ (1670 cm^{-1}, 1456 cm^{-1}), adsorbed NO_2 (1632 cm^{-1}), bidentate nitrate (1600 cm^{-1}), monodentate nitrate (1525 cm^{-1}) and NH_4NO_3 species (1303 cm^{-1}) presenting on the catalyst. The intensities of peaks ascribed to NH_4^+ and NH_4NO_3 species are greatly stronger than those of CeTi, indicating that a large amount of NH_4^+ and NH_4NO_3 are generated on the surface of SmCeTi catalyst. The *in situ* DRIFTS spectra of NO + O_2 adsorption experiment certificate that the doping of Sm into the CeTi can improve the adsorption ability of nitrate/nitrite species efficiently (Fig. 9), which should contribute to the large production of NH_4NO_3 species in NH_3 + NO + O_2 reaction. The peaks intensities of the NH_4NO_3 species is even strong at 300 °C. Interestingly, the activity of the catalyst is not affected by the appearance of large amount of NH_4NO_3, and the activity of SmCeTi catalyst is obviously higher than that of CeTi catalyst. Thus, the generation of NH_4^+ and NH_4NO_3 may be beneficial for the enhancement of the activity [9,21].

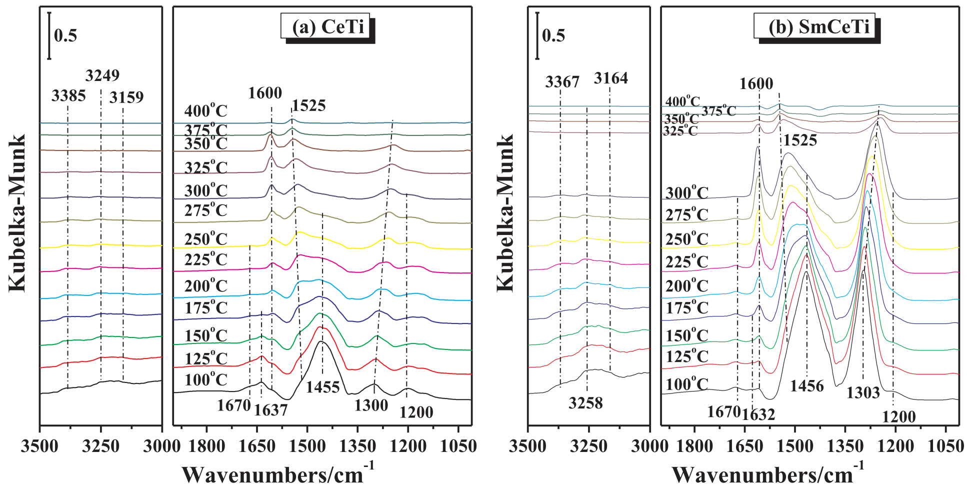

Fig. 11. *In situ* DRIFTS spectra of CeTi (a) and SmCeTi (b) in a flow of NH_3+NO + O_2 from 100 to 400 °C with a temperature interval of 25 °C.

3.5.5. Possible mechanism of the CeTi and SmCeTi catalysts in the NH_3-SCR reaction

A possible mechanism for the NO + O_2+NH_3 reaction on the CeTi catalyst is firstly proposed based on the above results. Brønsted acid sites are considered as the main active-sites, which is important for the NH_4^+ formation [8]. NO would be oxidized to NO_2 during the reaction process, and the oxidation of NO to NO_2 is generally thought to be one of an significant reaction step to promote NO_x reduction. Combined the single NH_3 and single NO adsorption spectra, the reduction of NO to N_2 in the NH_3-SCR reaction on CeTi surface is suggested mainly following Eqs. (5)–(8) [17,55,59,60]. NH_3 and NO species will be activated forming NH_4^+ and NO_2 on the CeTi catalysts, and then SCR reaction can occur between the NH_4^+ and NO_2 species.

$$2NH_3 \rightarrow 2NH_{3(a)} \tag{5}$$

$$2NH_{3(a)} + 2H^+ \rightarrow 2NH_4^+ \tag{6}$$

$$NO + 1/2O_2 \rightarrow NO_2 \tag{7}$$

$$NO_2 + 2NH_4^+ \rightarrow NO_2[NH_4^+]_2 + NO \rightarrow\cdots\rightarrow N_2 + 3H_2O + 2H^+ \tag{8}$$

It is reported by researchers that doping of Cu to CeO_2-TiO_2 mixed oxide catalysts can effectively improve the NH_3-SCR reaction performance due to the formation of $Cu^{2+}+Ce^{3+} \rightleftharpoons Cu^{+}+Ce^{4+}$ redox cycle [57]. In addition, the introduction of Fe, Ni, Sn *etc.* into the CeO_2-TiO_2 also can improve the NH_3-SCR reactivity, which is also attributed to the presence of $M^{n+}+Ce^{3+} \rightleftharpoons M^{(n-1)+}+Ce^{4+}$ (M = Fe, Ni, Sn *etc.*) [20,56,61]. In this work, it can be known from the XPS and DFT calculation results that the introduction of Sm into CeTi results in the electron transferring between Sm^{2+}/Sm^{3+} and Ce^{4+}/Ce^{3+} (*i.e.* $Ce^{4+}+Sm^{2+} \rightleftharpoons Ce^{3+}+Sm^{3+}$). Through this process, more Ce^{3+} is produced, which could induce the charge imbalance, oxygen vacancies and unsaturated chemical bonds on SmCeTi surface. From the results of *in situ* DRIFTS and literatures, it can be concluded that NO_x species may be reduced by NH_3 to form N_2 through several different pathways. Firstly, similar to that over the CeTi catalyst (eq.(8)), the NO_2 can react with NH_4^+ producing N_2 and H_2O. Secondly, the *in situ* DRIFTS spectra of NO + O_2 adsorption experiment certificate that doping of Sm into the CeTi can promote the formation of nitrate/nitrite species efficiently, and further produce the NH_4NO_3 species in NH_3+NO + O_2 condition. Gaseous NO and NH_3 may react with NH_4NO_3 to generate N_2 and H_2O (eq.(10)) [9]. Thirdly, NH_2 species, which are intermediates of ammonia activation, will be generated with the temperature increasing (Fig. 8**(b)**) on SmCeTi surface. Then, the NH_2 can react with gaseous NO producing N_2 and H_2O (eq.(12)). Therefore, the Sm species doped into the CeTi catalyst can lead the appearance of new active intermediates ($NH_{2(ad)}$), which enhance the catalytic activity of SmCeTi catalyst. The above results all suggest that NH_3 activation is an important process, and the NH_3-SCR reaction on the CeTi and SmCeTi catalysts is largely dominated by the E-R mechanism.

$$NO_{3(ad)}^- + NH_4^+ \rightarrow NH_4NO_3 \tag{9}$$

$$1/2NH_4NO_3 + NO + NH_3 \rightarrow 3/2N_2 + 5/2H_2O \tag{10}$$

$$NH_{3(ad)} \rightarrow NH_{2(ad)} + H^+ \tag{11}$$

$$NH_{2(ad)} + NO \rightarrow NH_2NO \rightarrow N_2 + H_2O \tag{12}$$

3.6. Insight into the SO_2 tolerance of the catalysts

The CeTi-U and SmCeTi-U catalysts were analyzed by TG-DSC, as shown in Fig. 12, to study the generated species left on the surface of catalysts in the NH_3-SCR reaction with the appearance of SO_2. The weight losses of two samples can mainly be divided into three steps. Step I (below 200 °C) is mainly related to the loss of adsorbed H_2O on the surface of samples [35,62]. Step II (200–550 °C) is caused by the decomposition of $(NH_4)_2SO_4$ and NH_4HSO_4 in N_2 purge [5,35]. For the CeTi-U catalyst, the percentage of weight loss in Step II is ~1.5%, while it is ~1.1% for SmCeTi-U catalyst, suggesting that the amounts of generated $(NH_4)_2SO_4$ and NH_4HSO_4 species in CeTi-U catalyst are higher than that in SmCeTi-U catalyst. The TG profiles of catalysts show a considerable decrease in Step III. Poston et al. [63] reported that the $Ce(SO_4)_2$ and $Sm_2(SO_4)_3$ species will decompose when the temperature is higher than 700 °C. Thence, Step III is attributed to the $Ce(SO_4)_2$ and/or $Sm_2(SO_4)_3$ decomposition. As can be seen, the weight loss of CeTi-U catalyst is 8.9%, which is higher than that of SmCeTi-U catalyst (6.5%). The results suggest the surface sulfate species of SmCeTi-U catalyst is lower than that of CeTi-U catalyst, and the addition of Sm to CeTi catalyst enhances the ability of sulfation resistance of catalyst.

Fig. 13 shows the *in situ* DRIFT spectra of SO_2+O_2 adsorbed on CeTi and SmCeTi catalysts at 250 °C as a function of time. The DRIFT spectra of SO_2+O_2 adsorption on CeTi (Fig. 13**(a)**) exhibit several peaks at 1341 cm^{-1} (S═O), 1293 cm^{-1} (S—O), 1084 cm^{-1} (S—O), and 1023 cm^{-1} (S—O), and the intensities increase with time proceeding, which demonstrates the formation of surface sulfate species [25,64]. According to the reported results, the peaks in the range of 1150-1200 cm^{-1} for the CeO_2, CeZr and CeTi samples are ascribed to the sulfates located in bulk or subsurface of CeO_2 and CeO_2 based solid solution (bulk or bulk-like sulfates) [25,65,66]. Because no bulk sulfate species are detected by XRD, so the peak at 1161 cm^{-1} suggests the bulk-like sulfate species forming on the CeTi catalyst surface. In addition, the peak at 1620 cm^{-1} is assigned to adsorbed H_2O generated

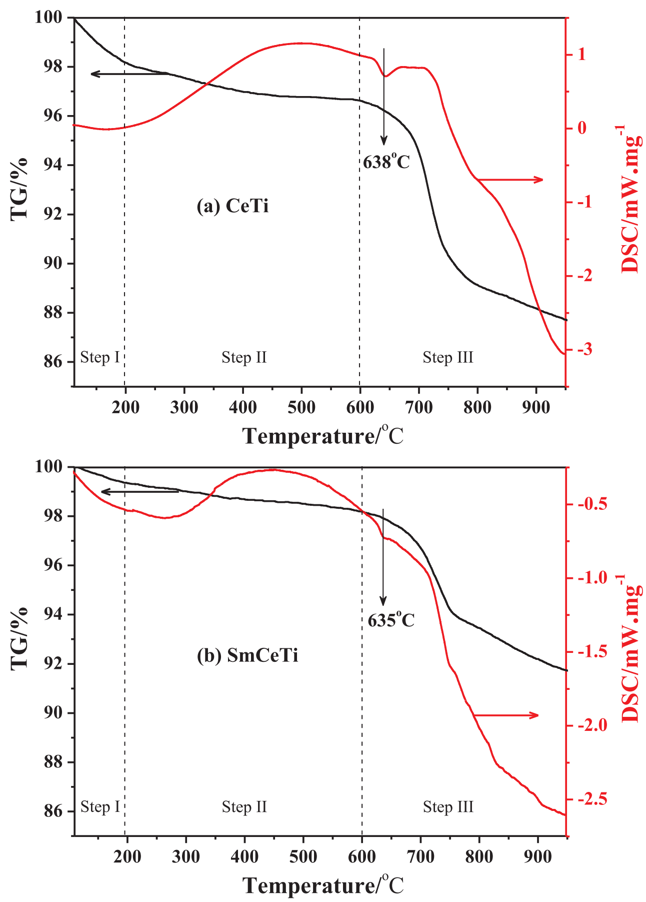

Fig. 12. TG-DSC curves of CeTi-U (a) and SmCeTi-U (b).

from the SO_2 and surface −OH groups [62]. Overall, both surface and bulk-like sulfate species can form on CeTi catalyst surface with the appearance of SO_2+O_2. For the SmCeTi catalysts, the peaks representing the surface sulfate species (1347, 1292, 1085 and 1046 cm^{-1}) can also be observed in the DRIFT spectra (Fig. 13**(b)**). However, no bulk-like sulfate species (peak at approximately 1150-1200 cm^{-1}) forms on the surface of SmCeTi catalysts. The results reveal that the reaction between SO_2 and Ce species is suppressed probably by the introduced Sm species, and the bulk-like sulfates forms on SmCeTi catalyst more difficultly than that on CeTi catalyst. In addition, the DRIFT spectrum of SmCeTi-U sample suggests no bulk-like sulfate species are detected (**Fig. S4**), which further confirms the effect of Sm doping.

Ce-O-Ti is reported to be the active species of the NH_3-SCR reaction [24,49]. According to the previous reported results, there are mainly two different ways for SO_2 poisoning of catalysts [35,67,68]. SO_2 could be oxidized to SO_3 on the surface of catalysts, and the SO_3 will react with gaseous species (H_2O and NH_3) or the catalyst to form NH_4HSO_4 or metal sulfates. Both of them can cover the active sites and cause the decrease of catalytic activity of catalysts. To investigate the reason of SO_2 poisoning of the catalyst, the NH_3-SCR reactivity of 5 wt.% NH_4HSO_4 loaded CeTi and SmCeTi was tested. As shown in **Fig. S5**, there is no significant effect of NH_4HSO_4 on the catalytic activity of CeTi and SmCeTi samples, when the temperature is above 250 °C. This indicates that the NH_4HSO_4 will decompose on the catalysts surface when the temperature is higher than 250 °C, and the decrease of catalytic activity for the CeTi and SmCeTi catalysts is not induced by the deposition of NH_4HSO_4 on the surface of CeTi and SmCeTi catalysts above 250 °C. Consequently, it seems reasonable to propose that the deactivation of CeTi catalyst is mainly caused by the metal sulfation (cerium sulfate [25]). Furthermore, the catalysts are pretreated with SO_2+O_2 (250 °C, 1000 ppm SO_2, 5 vol.% O_2, 1 h) to support our deduction. As shown in **Fig. S6**, after pretreated by SO_2+O_2, the activity of the CeTi catalyst decreases more significantly than that of the SmCeTi catalyst. The results suggest metal sulfation will decrease the activity of catalysts, and the introduction of Sm may inhibit the deep sulfation of catalysts.

The reason of the significant SO_2 resistance of SmCeTi catalyst may be ascribed to the formation of $Ce^{4+}+Sm^{2+} \rightleftharpoons Ce^{3+}+Sm^{3+}$ circles [5]. For the CeTi catalyst, as shown in Scheme 2, the electron of adsorbed SO_2 can transfer to Ce^{4+}, which make the SO_2 oxidize to SO_3 and produce bulk-like sulfates. After the introduction of Sm, the electron transfer from SO_2 to Ce^{4+} is inhibited by the electron transfer of $Sm^{2+} \rightarrow Ce^{4+}$, and the generation of sulfate species is consequently suppressed on the surface of SmCeTi catalysts. Thus, much fewer cerium sulfate species is produced and the Ce-O-Ti active sites are preserved, and the SmCeTi catalysts show excellent SO_2 resistance ability.

4. Conclusions

In summary, Sm doping into CeO_2-TiO_2 mixed oxides significantly improves the NH_3-SCR reactivity and SO_2 tolerance of catalysts. The reducibility and OSC of CeTi catalyst are promoted by the addition of Sm species, which is beneficial for improving the activity of catalyst. The SmCeTi catalysts exhibit the good activity is attributed to the appropriate balance of the acidity and redox property. The NH_3-SCR reaction on the surface of both catalysts proceeds obey the E-R mechanism. The electron transferring between Sm^{2+}/Sm^{3+} and Ce^{4+}/Ce^{3+} improves the adsorbed ability of nitrate species. In addition, the doping of Sm to CeTi induces the facile switch between Ce^{4+} and Ce^{3+} species and promotes the production of NH_3 to NH_2. Thus, new reaction

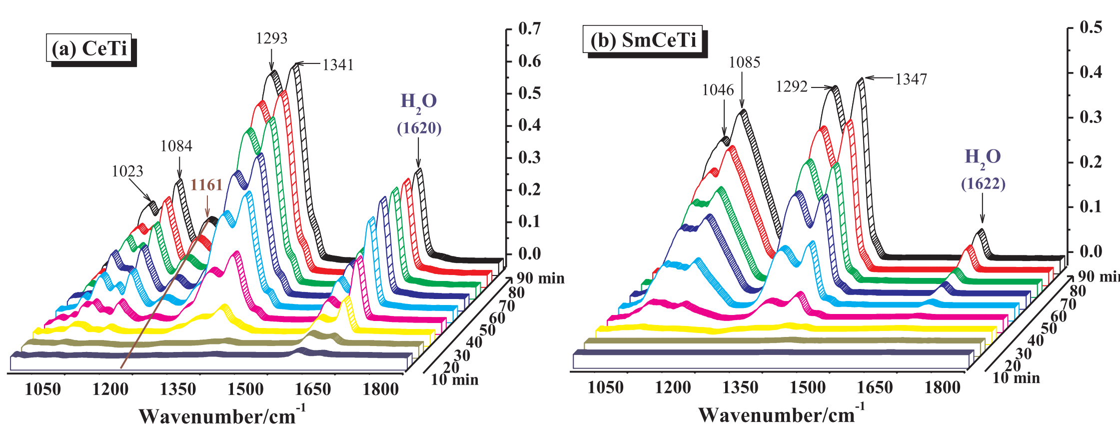

Fig. 13. *In situ* DRIFT SO_2+O_2 adsorption spectra over CeTi (a) and SmCeTi (b) at 250 °C as a function of time.

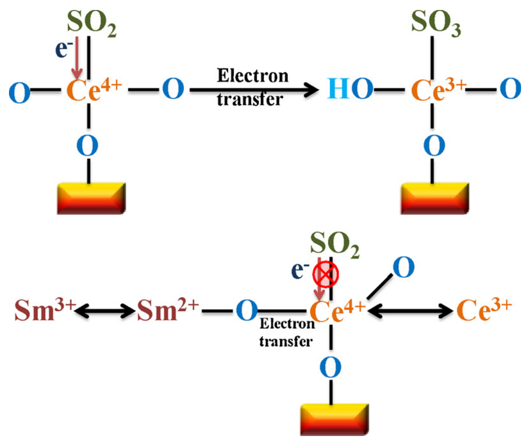

Scheme 2. Diagram for the suppressed oxidation of SO_2 to SO_3 on SmCeTi.

pathways may proceed on the SmCeTi catalyst in the NH_3-SCR reaction. The deposition rate of sulphate species on the surface of SmCeTi catalyst is lowered and the SO_2 tolerance of SmCeTi catalyst is distinctly enhanced by samarium doping, which is ascribed to the inhibition of the oxidation of SO_2 to SO_3 due to the suppression of electron transferring from adsorbed SO_2 to Ce^{4+}. Our work provides a useful strategy for the preparation of new mixed metal oxides catalysts with good activity and SO_2 tolerance ability in the NH_3-SCR reaction.

Acknowledgements

This work was supported by the National Natural Science Foundation of China (21677069 and 21403134), Natural Science Foundation of Shandong (ZR2017BB050), and Jinan Program of Science and Technology (201401240). The numerical calculations in this paper were performed on the computing system in the Computing Center of the School of Physics and Electronic Engineering of Taishan University of China.

Appendix A. Supplementary data

Supplementary material related to this article can be found, in the online version, at doi:https://doi.org/10.1016/j.apcatb.2018.12.001.

References

[1] L. Zong, G. Zhang, J. Zhao, F. Dong, J. Zhang, Z. Tang, Chem. Eng. J. 343 (2018) 500–511.
[2] L. Zong, G. Zhang, H. Zhao, J. Zhang, Z. Tang, Chem. Eng. J. 354 (2018) 295–303.
[3] X. Wang, Y. Shi, S. Li, W. Li, Appl. Catal. B: Environ. 220 (2018) 234–250.
[4] J. Arfaoui, A. Ghorbel, C. Petitto, G. Delahay, Appl. Catal. B: Environ. 224 (2018) 264–275.
[5] C. Sun, H. Liu, W. Chen, D. Chen, S. Yu, A. Liu, L. Dong, S. Feng, Chem. Eng. J. 347 (2018) 27–40.
[6] S. Yang, S. Xiong, Y. Liao, X. Xiao, F. Qi, Y. Peng, Y. Fu, W. Shan, J. Li, Environ. Sci. Technol. 48 (2014) 10354–10362.
[7] X.S. Huang, G. Zhang, G. Lu, Z. Tang, Catal. Surv. Asia 22 (2017) 1–19.
[8] N.-Y. Topsøe, Science 265 (1994) 1217–1219.
[9] C. Ciardelli, I. Nova, E. Tronconi, D. Chatterjee, B. Bandl-Konrad, Chem. Commun. (Camb.) (2004) 2718–2719.
[10] H. Hu, S. Cai, H. Li, L. Huang, L. Shi, D. Zhang, ACS Catal. 5 (2015) 6069–6077.
[11] L. Ma, C.Y. Seo, M. Nahata, X. Chen, J. Li, J.W. Appl. Catal. B: Environ., 232 (2018) 246-259.
[12] Z. Chen, Q. Yang, H. Li, X. Li, L. Wang, S. Chi Tsang, J. Catal. 276 (2010) 56–65.
[13] E. Park, M. Kim, H. Jung, S. Chin, J. Jurng, ACS Catal. 3 (2013) 1518–1525.
[14] Q. Yan, S. Chen, C. Zhang, Q. Wang, B. Louis, Appl. Catal. B: Environ. 238 (2018) 236–247.
[15] L.J. France, Q. Yang, W. Li, Z. Chen, J. Guang, D. Guo, L. Wang, X. Li, Appl. Catal. B: Environ. 206 (2017) 203–215.
[16] L. Yan, Y. Liu, K. Zha, H. Li, L. Shi, D. Zhang, Catal. Sci. Technol. 7 (2017) 502–514.
[17] Z. Ma, X. Wu, Z. Si, D. Weng, J. Ma, T. Xu, Appl. Catal. B: Environ. 179 (2015) 380–394.
[18] S. Ali, L. Chen, F. Yuan, R. Li, T. Zhang, S.U.H. Bakhtiar, X. Leng, X. Niu, Y. Zhu, Appl. Catal. B: Environ. 210 (2017) 223–234.
[19] Y. Li, Y. Wan, Y. Li, S. Zhan, Q. Guan, Y. Tian, Appl. Catal. A Gen. 528 (2016) 150–160.
[20] G. Zhang, W. Han, H. Zhao, L. Zong, Z. Tang, Appl. Catal. B: Environ. 226 (2018) 117–126.
[21] L. Chen, Z. Si, X. Wu, D. Weng, ACS Appl. Mater. Interfaces 6 (2014) 8134–8145.
[22] L. Li, L. Zhang, K. Ma, W. Zou, Y. Cao, Y. Xiong, C. Tang, L. Dong, Appl. Catal. B: Environ. 207 (2017) 366–375.
[23] Z. Zhang, L. Chen, Z. Li, P. Li, F. Yuan, X. Niu, Y. Zhu, Catal. Sci. Technol. 6 (2016) 7151–7162.
[24] P. Li, Y. Xin, Q. Li, Z. Wang, Z. Zhang, L. Zheng, Environ. Sci. Technol. 46 (2012) 9600–9605.
[25] W. Xu, H. He, Y. Yu, J. Phy. Chem. C 113 (2009) 4426–4432.
[26] J. Liu, X. Li, Q. Zhao, J. Ke, H. Xiao, X. Lv, S. Liu, M. Tadé, S. Wang, Appl. Catal. B: Environ. 200 (2017) 297–308.
[27] Y. Shu, H. Sun, X. Quan, S. Chen, J. Phy. Chem. C 116 (2012) 25319–25327.
[28] P. Yang, C. Lu, N. Hua, Y. Du, Mater. Lett. 57 (2002) 794–801.
[29] D. Meng, W. Zhan, Y. Guo, Y. Guo, L. Wang, G. Lu, ACS Catal. 5 (2015) 5973–5983.
[30] D. Meng, W. Zhan, Y. Guo, Y. Guo, Y. Wang, L. Wang, G. Lu, J. Mol. Catal. A Chem. 420 (2016) 272–281.
[31] G. Kresse, J. Hafner, Ab initio, Phys. Rev. B 49 (1994) 14251–14269.
[32] G. Kresse, J. Furthmüller, Phy. Rev. B 54 (1996) 11169–11186.
[33] G. Kresse, D. Joubert, Phy. Rev. B 59 (1999) 1758–1775.
[34] J.P. Perdew, K. Burke, M. Ernzerhof, Phy. Rev. Lett. 77 (1996) 3865–3868.
[35] L. Zhang, L. Li, Y. Cao, X. Yao, C. Ge, F. Gao, Y. Deng, C. Tang, L. Dong, Appl. Catal. B: Environ. 165 (2015) 589–598.
[36] W. Cai, Q. Zhong, W. Zhao, Y. Bu, Appl. Catal. B: Environ. 158-159 (2014) 258–268.
[37] J.G. Kang, B.K. Min, Y. Sohn, J. Mater. Sci. 50 (2014) 1958–1964.
[38] Z. Liu, J. Zhu, J. Li, L. Ma, S.I. Woo, ACS Appl. Mater. Interfaces 6 (2014) 14500–14508.
[39] X. Cheng, X. Zhang, D. Su, Z. Wang, J. Chang, C. Ma, Appl. Catal. B: Environ. 239 (2018) 485–501.
[40] X. Zhao, L. Huang, H. Li, H. Hu, X. Hu, L. Shi, D. Zhang, Appl. Catal. B: Environ. 183 (2016) 269–281.
[41] B.T. Sone, E. Manikandan, A. Gurib-Fakim, M. Maaza, J. Alloys Compds. 650 (2015) 357–362.
[42] S. Yang, Y. Guo, H. Chang, L. Ma, Y. Peng, Z. Qu, N. Yan, C. Wang, J. Li, Appl. Catal. B: Environ. 136-137 (2013) 19–28.
[43] W. Li, C. Zhang, X. Li, P. Tan, A. Zhou, Q. Fang, G. Chen, Chin. J. Catal. 39 (2018) 1653–1663.
[44] Z. Lian, F. Liu, W. Shan, H. He, J. Phy. Chem. C 121 (2017) 7803–7809.
[45] B. Li, Z. Ren, Z. Ma, X. Huang, F. Liu, X. Zhang, H. Yang, Catal. Sci. Technol. 6 (2016) 1719–1725.
[46] S. Watanabe, X. Ma, C. Song, J. Phy. Chem. C 113 (2009) 14249–14257.
[47] D. Chen, D. He, J. Lu, L. Zhong, F. Liu, J. Liu, J. Yu, G. Wan, S. He, Y. Luo, Appl. Catal. B: Environ. 218 (2017) 249–259.
[48] A. Rangaswamy, P. Sudarsanam, B.M. Reddy, J. Rare Earths 33 (2015) 1162–1169.
[49] J. Ding, Q. Zhong, S. Zhang, Ind. Eng. Chem. Res. 54 (2015) 2012–2022.
[50] C. Li, Z. Huang, Y. Chen, X. Liu, J. Chen, W. Qu, Z. Ma, X. Tang, ChemCatChem 10 (2018) 3990–3994.
[51] D. Wang, Y. Peng, Q. Yang, F. Hu, J. Li, J. Crittenden, Catal. Today (2018), https://doi.org/10.1016/j.cattod.2018.07.048.
[52] L. Chen, F. Yuan, Z. Li, X. Niu, Y. Zhu, Chem. Eng. J. 354 (2018) 393–406.
[53] F. Liu, H. He, Catal. Today 153 (2010) 70–76.
[54] P. Hobza, Z. Havlas, Chem. Rev. 100 (2000) 4253–4264.
[55] L. Chen, J. Li, M. Ge, Environ. Sci. Technol. 44 (2010) 9590–9596.
[56] Z. Liu, Y. Liu, B. Chen, T. Zhu, L. Ma, Catal. Sci. Technol. 6 (2016) 6688–6696.
[57] Z. Liu, Y. Yi, J. Li, S.I. Woo, B. Wang, X. Cao, Z. Li, Chem. Commun. (Camb.) 49 (2013) 7726–7728.
[58] P.R. Ettireddy, N. Ettireddy, T. Boningari, R. Pardemann, P.G. Smirniotis, J. Catal. 292 (2012) 53–63.
[59] X. Xiao, S. Xiong, Y. Shi, W. Shan, S. Yang, J. Phy. Chem. C 120 (2016) 1066–1076.
[60] R.Q. Long, R.T. Yang, J. Catal. 190 (2000) 22–31.
[61] Z. Liu, H. Liu, X. Feng, L. Ma, X. Cao, B. Wang, Mol. Catal. 445 (2018) 179–186.
[62] R. Jin, Y. Liu, Y. Wang, W. Cen, Z. Wu, H. Wang, X. Weng, Appl. Catal. B: Environ. 148-149 (2014) 582–588.
[63] J.A. Poston, R.V. Siriwardane, E.P. Fisher, A.L. Miltz, Appl. Surf. Sci. 214 (2003) 83–102.
[64] U. Tumuluri, M. Li, B.G. Cook, B. Sumpter, S. Dai, Z. Wu, J. Phy. Chem. C 119 (2015) 28895–28905.
[65] M. Waqif, P. Bazin, O. Saur, J.C. Lavalley, G. Blanchard, O. Touret, Appl. Catal. B: Environ. 11 (1997) 193–205.
[66] T. Luo, R.J. Gorte, Appl. Catal. B: Environ. 53 (2004) 77–85.
[67] G. Busca, L. Lietti, G. Ramis, F. Berti, Appl. Catal. B: Environ. 18 (1998) 1–36.
[68] P. Forzatti, Appl. Catal. A Gen. 222 (2001) 221–236.